

# Anti-symmetric Compton scattering in LiNiPO<sub>4</sub>: Towards a direct probe of the magneto-electric multipole moment

## Journal Article

### Author(s):

Bhowal, Sayantika ; O'Neill, Daniel; Fechner, Michael; Spaldin, Nicola A.; Staub, Urs; Duffy, Jon; Collins, Stephen P.

### Publication date:

2021-11-01

### Permanent link:

<https://doi.org/10.3929/ethz-b-000517979>

### Rights / license:

[Creative Commons Attribution 4.0 International](#)

### Originally published in:

Open Research Europe 1, <https://doi.org/10.12688/openreseurope.13863.1>

### Funding acknowledgement:

810451 - Hidden, entangled and resonating orders/HERO (EC)



## RESEARCH ARTICLE

# Anti-symmetric Compton scattering in $\text{LiNiPO}_4$ : Towards a direct probe of the magneto-electric multipole moment

[version 1; peer review: 1 approved]

Sayantika Bhowal<sup>1\*</sup>, Daniel O'Neill<sup>2\*</sup>, Michael Fechner<sup>3\*</sup>, Nicola A. Spaldin<sup>1</sup>, Urs Staub<sup>4</sup>, Jon Duffy<sup>2</sup>, Stephen P. Collins<sup>5</sup>

<sup>1</sup>Materials Theory, ETH Zürich, Zurich, 8093, Switzerland

<sup>2</sup>Department of Physics, University of Warwick, Coventry, CV4 7AL, UK

<sup>3</sup>Condensed Matter Dynamics Department, Max Planck Institute for the Structure and Dynamics of Matter, Hamburg, 22761, Germany

<sup>4</sup>Swiss Light Source, Paul Scherrer Institute, Villigen, 5232, Switzerland

<sup>5</sup>Diamond Light Source, Didcot, Oxfordshire, OX11 0DE, UK

\* Equal contributors

**V1** First published: 01 Nov 2021, 1:132  
<https://doi.org/10.12688/openreseurope.13863.1>

Latest published: 01 Nov 2021, 1:132  
<https://doi.org/10.12688/openreseurope.13863.1>

## Abstract

Background: Magnetoelectric multipoles, which break both space-inversion and time-reversal symmetries, play an important role in the magnetoelectric response of a material. Motivated by uncovering the underlying fundamental physics of the magnetoelectric multipoles and the possible technological applications of magnetoelectric materials, understanding as well as detecting such magnetoelectric multipoles has become an active area of research in condensed matter physics. Here we employ the well-established Compton scattering effect as a possible probe for the magnetoelectric toroidal moments in  $\text{LiNiPO}_4$ .

Methods: We employ combined theoretical and experimental techniques to compute as well as detect the antisymmetric Compton profile in  $\text{LiNiPO}_4$ . For the theoretical investigation we use density functional theory to compute the anti-symmetric part of the Compton profile for the magnetic and structural ground state of  $\text{LiNiPO}_4$ . For the experimental verification, we measure the Compton signals for a single magnetoelectric domain sample of  $\text{LiNiPO}_4$ , and then again for the same sample with its magnetoelectric domain reversed. We then take the difference between these two measured signals to extract the antisymmetric Compton profile in  $\text{LiNiPO}_4$ .

Results: Our theoretical calculations indicate an antisymmetric Compton profile in the direction of the  $t_y$  toroidal moment in

## Open Peer Review

Reviewer Status

Invited Reviewers

1

version 1

01 Nov 2021

[report](#)

1. **Lars Nordstrom** , Uppsala University, Uppsala, Sweden

Any reports and responses or comments on the article can be found at the end of the article.

momentum space, with the computed antisymmetric profile around four orders of magnitude smaller than the total profile. The difference signal that we measure is consistent with the computed profile, but of the same order of magnitude as the statistical errors and systematic uncertainties of the experiment.

**Conclusions:** While the weak difference signal in the measurements prevents an unambiguous determination of the antisymmetric Compton profile in  $\text{LiNiPO}_4$ , our results motivate further theoretical work to understand the factors that influence the size of the antisymmetric Compton profile, and to identify materials exhibiting larger effects.

### Keywords

Magneto-electric toroidal moment, Compton scattering, Density functional theory, Lithium transition metal phosphate



This article is included in the [Excellent Science](#) gateway.

**Corresponding author:** Sayantika Bhowal ([sayantika.bhowal@mat.ethz.ch](mailto:sayantika.bhowal@mat.ethz.ch))

**Author roles:** **Bhowal S:** Formal Analysis, Investigation, Visualization, Writing – Original Draft Preparation; **O'Neill D:** Formal Analysis, Investigation; **Fechner M:** Conceptualization, Investigation, Writing – Review & Editing; **Spaldin NA:** Conceptualization, Resources, Supervision, Writing – Review & Editing; **Staub U:** Conceptualization, Investigation, Writing – Review & Editing; **Duffy J:** Conceptualization, Investigation, Methodology, Writing – Review & Editing; **Collins SP:** Conceptualization, Investigation, Methodology, Writing – Review & Editing

**Competing interests:** No competing interests were disclosed.

**Grant information:** This research was financially supported by the European Union's Horizon 2020 research, innovation programme under the grant agreement No 810451 (projectHERO), and by Eidgenössische Technische Hochschule Zürich.

**Copyright:** © 2021 Bhowal S *et al.* This is an open access article distributed under the terms of the [Creative Commons Attribution License](#), which permits unrestricted use, distribution, and reproduction in any medium, provided the original work is properly cited.

**How to cite this article:** Bhowal S, O'Neill D, Fechner M *et al.* **Anti-symmetric Compton scattering in  $\text{LiNiPO}_4$ : Towards a direct probe of the magneto-electric multipole moment** [version 1; peer review: 1 approved] Open Research Europe 2021, 1:132 <https://doi.org/10.12688/openreseurope.13863.1>

**First published:** 01 Nov 2021, 1:132 <https://doi.org/10.12688/openreseurope.13863.1>

## I. Plain language summary

Materials containing magnetic dipoles, made from the north and south poles of magnets, have been used for millennia for navigation (since they line up along the earth's magnetic fields), and in modern times for data storage (with their orientations representing the 1s and 0s of digital electronics). Analogous to these magnetic dipoles with their north and south poles are electric dipoles, made of positive and negative charges. Materials containing both electric and magnetic dipoles are rather rare and are an active area of research both because of their potential technological applications in memory, logic or sensor components and because of their intriguing fundamental physics. In particular, the basic electro-magnetic building blocks of such materials, made of composites of electric and magnetic dipoles, are of huge interest, and are likely related to exotic behaviors such as superconductivity (the conduction of electricity with no resistance) and other unusual electrical and magnetic properties. In this research, we describe an advanced experimental technique for detecting one of these composites – the so-called magnetoelectric multipole moment – using high-energy x-ray beams.

## II. Introduction

Magnetoelectric (ME) multipoles are key to understanding the linear ME response in solids, in which an applied electric field induces a linear order magnetization, and vice versa. In particular, the second-rank ME multipole tensor, defined as  $\mathcal{M}_{ij} = \int r_i \mu_j(\vec{r}) d^3r$ <sup>1,2</sup>, where  $\vec{\mu}(\vec{r})$  is the magnetization density, has the same symmetry as the linear ME response tensor. Both are only non-zero when space-inversion ( $\mathcal{I}$ ) and time-reversal ( $\mathcal{T}$ ) symmetries are broken simultaneously, and there is a one-to-one correlation between their components. For example, materials with an antisymmetric off-diagonal linear ME response also have non-zero antisymmetric off-diagonal elements in their  $\mathcal{M}_{ij}$  tensor<sup>3</sup>.

The ME multipole  $\mathcal{M}_{ij}$  tensor can be decomposed into three irreducible (IR) components, the ME monopole, ME dipole (toroidal) moment, and ME quadrupole moment, as summarized in Table I<sup>1,2</sup>. In the present work, we are particularly interested in the ME toroidal moment  $\vec{t} = \frac{1}{2} \int \vec{r} \times \vec{\mu}(\vec{r}) d^3r$ , the components of

which form the antisymmetric off-diagonal elements of the multipole tensor  $\mathcal{M}_{ij}$ ,

$$t_i = \frac{1}{2} \epsilon_{ijk} \mathcal{M}_{jk} . \quad (1)$$

The ME toroidal moment has been proposed as the order parameter for a form of hidden ferroic order, known as *ferrotoroidic*, to complete the set of primary ferroics with the existing established ferromagnetism, ferroelectricity, and ferroelasticity<sup>1,4,5</sup>. This proposal motivated considerable interest in ME toroidal moments in solids, leading to experimental efforts to detect them using resonant x-ray diffraction<sup>6–10</sup>, magneto chiral dichroism<sup>11,12</sup>, and optical measurements<sup>13</sup>, as well as to image ferrotoroidic domains<sup>5</sup>. While a theory of *toroidization* (toroidal moment per unit volume) in periodic solids has been developed<sup>14</sup>, a direct and quantifiable link of detected signals from toroidal moments to the underlying electronic structure is still lacking.

Recently, the occurrence of an antisymmetric component in the Compton scattering profile, which measures the electron momentum density  $\rho(\vec{p})$ , was proposed as a possible direct probe of the ME toroidal moment<sup>15</sup>. For materials that are symmetric in either or both of  $\mathcal{I}$  and  $\mathcal{T}$ , the Compton profile,  $J(p)$ , which is a projection of electron momentum density of the form  $J(p_z) = \int \rho(\vec{p}) dp_x dp_y$ , is symmetric in momentum space, because under both  $\mathcal{T}$  and  $\mathcal{I}$ ,  $\vec{p} \rightarrow -\vec{p}$ . For materials that lack both  $\mathcal{I}$  and  $\mathcal{T}$  symmetries, however, an antisymmetric contribution to the Compton profile is allowed, suggesting Compton scattering as a sensitive probe of atomic-scale magnetoelectric properties. A first investigation was made using magnetoelectric GaFeO<sub>3</sub><sup>15</sup>, for which a density functional study of the ideal material predicted a measurable asymmetry. The measured Compton asymmetry, however, was within the experimental uncertainty, possibly due to the well-known inter-site mixing of Ga and Fe in GaFeO<sub>3</sub>, and so no clear assignment of a toroidal moment could be made.

Here, we present a combined theoretical and experimental Compton scattering study of a magnetoelectric material, lithium nickel phosphate, that has no reported tendency to site disorder. LiNiPO<sub>4</sub> is an anti-ferromagnetic insulator, which shows

**Table I.** The three irreducible components of the magnetoelectric (ME) multipole tensor  $\mathcal{M}_{ij}$  that contribute to the second order term  $\mathcal{E}_{int}^{(2)}$  in the multipole expansion of the interaction energy in presence of an external magnetic field  $\vec{H}$ .

ME multipole	ME monopole ( $a$ )	ME toroidal moment ( $\vec{t}$ )	ME quadrupole moment ( $q_{ij}$ )
Definition	$a = \frac{1}{3} \mathcal{M}_{ii} = \frac{1}{3} \int \vec{r} \cdot \vec{\mu}(\vec{r}) d^3r$	$t_i = \frac{1}{2} \epsilon_{ijk} \mathcal{M}_{jk} = \frac{1}{2} \int \vec{r} \times \vec{\mu}(\vec{r}) d^3r$	$q_{ij} = \frac{1}{2} \int (r_i \mu_j + r_j \mu_i - \frac{2}{3} \delta_{ij} \vec{r} \cdot \vec{\mu}) d^3r$
Rank	0 (scalar)	1 (vector)	2 (symmetric traceless tensor)
$\mathcal{E}_{int}^{(2)} = -\int r_i \mu_j(\vec{r}) \partial_i H_j(\vec{0}) d^3r$	$-a(\vec{\nabla} \cdot \vec{H})_{\vec{r}=0}$	$-\vec{t} \cdot (\vec{\nabla} \times \vec{H})_{\vec{r}=0}$	$-q_{ij}(\partial_i H_j + \partial_j H_i)$

an off-diagonal linear ME response<sup>16–18</sup> and hosts a ME toroidal moment<sup>2</sup> in its magnetic ground state. (Note that many magnetic-field induced magnetic transitions have recently been identified, resulting in other phases with linear and quadratic ME effects which we do not treat here<sup>18</sup>.) Our calculations using density functional theory (DFT) indeed show the presence of an antisymmetric Compton profile along the  $y$  direction in momentum space, consistent with the presence of the ME toroidal moment component  $t_y$  in  $\text{LiNiPO}_4$ . The calculated intensity of the antisymmetric part of the profile is about four orders of magnitude smaller than that of the corresponding total profile. Our measured antisymmetric signal is of the same order of magnitude as our computed value, but is also of the same order of magnitude as the statistical errors and systematic uncertainties of the experiments. Our main finding, therefore, is that, while an antisymmetric Compton scattering would indeed indicate the existence of a magnetoelectric multipole in a material, improvements in the experimental sensitivity and/or identification of materials with a larger response will be necessary for an unambiguous determination.

We organize the paper as follows. In [section III](#), we provide a detailed description of the crystal structure of  $\text{LiNiPO}_4$  and discuss the theoretical and experimental methods used in the present work to analyze its Compton profile. This is followed by the discussion of our results in [section IV](#). Here, we first discuss the density functional results and the experimental results individually and, then, compare our theory and experiments in order to gain insight into the measured Compton profile in  $\text{LiNiPO}_4$ . We also discuss the possible roles of domain averaging and convolution of the profile in reducing the antisymmetric signal in the measurements. Finally, we summarize our findings in [section V](#).

### III. Methods

In this section, we discuss the crystal structure of  $\text{LiNiPO}_4$ , followed by the theoretical and experimental methods that were employed in the present work to obtain and study the Compton profile of the material.

#### A. Crystal structure

$\text{LiNiPO}_4$  crystallizes in the orthorhombic  $Pnma$  structure, with the point group symmetry  $D_{2h}^{19}$ . The unit-cell structure is shown in [Figure 1](#). As seen from this figure, the crystal structure consists of distorted  $\text{NiO}_6$  octahedra, which are connected to each other by  $\text{PO}_4$  tetrahedral units. The unit cell consists of four formula units, with the four Ni atoms occupying the Wyckoff positions  $4c$ . In contrast to the previously studied  $\text{GaFeO}_3$ , the crystal structure of  $\text{LiNiPO}_4$  has inversion  $\mathcal{I}$  symmetry in the absence of magnetic ordering. The magnetic arrangement at the Ni sites in the ground state breaks both  $\mathcal{I}$  and time-reversal  $\mathcal{T}$  symmetries, leading to a linear ME effect and a non-zero toroidal moment. The combined  $\mathcal{IT}$  symmetry remains preserved in this magnetic ground state.

#### B. Computational methods

The electronic structure, the antisymmetric Compton profile, and the ME multipoles for  $\text{LiNiPO}_4$  are obtained using the

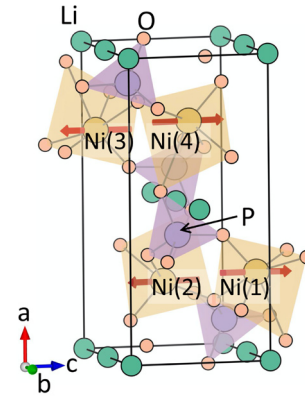


**Figure 1.** The crystal and magnetic structure of  $\text{LiNiPO}_4$ . The red arrows denote the spin moment at the Ni sites corresponding to the magnetic ground state with  $Pnm'a$  symmetry.

linearized augmented plane wave (LAPW) method of density functional theory as implemented in the ELK code (version: 4.0.15)<sup>20,21</sup>. Within the density functional theory method, the single particle Kohn-Sham equations are solved to obtain the band energies, which are used later to compute the electron momentum density. Spin-orbit coupling (SOC) is included explicitly in the calculations. A local Hubbard  $U$  correction of  $U_{\text{eff}} = U - J = 4.25$  eV is applied to the Ni  $3d$  electrons, within the LDA+SOC+ $U$  formalism. We use the default ELK atomic species files in calculations, treating Li:  $1s^2 2s^1$ , Ni:  $3p^6 3d^8 4s^2$ , P:  $3s^2 3p^3$ , and O:  $2s^2 2p^4$  electrons as valence electrons. The corresponding muffin-tin radii for Li, Ni, P, and O are taken to be 2.0, 2.4, 2.2, and 1.8 a.u. respectively. In order to achieve self consistency, we use a basis set of  $l_{\text{max(apw)}} = 8$ , we sample the Brillouin zone with a  $3 \times 6 \times 6$  k-point mesh, and take the product of the muffin-tin radius and the maximum reciprocal lattice vector to be 7. The calculations are carried out using the reported relaxed atomic positions calculated in  $\text{LiNiPO}_4$ <sup>2</sup>.

Once self-consistency is achieved, we compute the electron momentum density using the same ELK code (version: 4.0.15). This is further projected onto the selected momentum directions ( $\vec{p}$ ) in order to obtain the desired Compton profile  $J(\vec{p})$ <sup>21</sup>. Next, we separate out the computed profile into symmetric  $J^s(\vec{p})$  and antisymmetric  $J^a(\vec{p})$  parts using the following relation,

$$\begin{aligned} J(\vec{p}) &= 2^{-1}[J(\vec{p}) + J(-\vec{p})] + 2^{-1}[J(\vec{p}) - J(-\vec{p})] \\ &= J^s(\vec{p}) + J^a(\vec{p}) \end{aligned} \quad (2)$$

Additional calculations with a denser  $5 \times 10 \times 10$  k-point mesh confirm the convergence of each of the parts,  $J^s(\vec{p})$  and  $J^a(\vec{p})$ . We normalize both profiles to the total number of valence electrons per formula unit of  $\text{LiNiPO}_4$ , 48, and add the isotropic core contribution to the symmetric part to obtain the total calculated Compton profile, which should be comparable with the measured profile. The core contribution is obtained from the Hartree-Fock calculations of Biggs *et al.*<sup>22</sup>. To compare the computed antisymmetric Compton profile with the measured

value, we further convolute the computed profile with a Gaussian of full-width at half maximum (FWHM) = 0.44 a.u. to mimic the experimental momentum resolution, which is dominated by the detector energy resolution of  $\Delta E/E \sim 7 \times 10^{-3}$ .

We calculate the ME multipoles in the sphere around the Ni sites (referred to as the atomic-site contributions in Refs. 2 and 14) by decomposing the density matrix  $\rho_{lm,l'm'}$  as described in Ref. 2. The parity-odd tensor moments have contributions only from the odd  $l - l'$  terms, i.e.,  $l$  must be different from  $l'$ ; for the case of Ni with its valence  $s$ ,  $p$  and  $d$  electrons, this means that we include the  $p - s$  and  $p - d$  matrix element contributions, which provide the measure of the multipoles.

Note that the computed multipoles are in  $\mu_B$  unit and we label them as  $\tilde{t}_y$ ,  $\tilde{q}_{xz}$  etc. in Table II.

### C. Experimental techniques

Our experiment, carried out on BL08W(A) at SPring-8, utilized the Warwick University superconducting magnet to provide a 7T field perpendicular to the beam, coupled with a high voltage (600V), applied perpendicular to the beam and magnetic field. The experimental set up is shown schematically in Figure 2. The sample was cooled through the ordering phase transition to around T=10K, while applying the magnetic and electric fields simultaneously. Then the cycle was repeated in an + - - + magnetic field sequence, with the same electric

**Table II.** The computed magnitudes and relative signs of magnetoelectric (ME) multipoles and magnetic moments at the Ni site (Wyckoff position 4c) corresponding to the  $Pnm'a$  magnetic structure. The Ni(1), Ni(2), Ni(3), and Ni(4) atoms are indicated in Figure 1.

ME multipoles	Magnitude ( $10^{-3}\mu_B$ )	Relative orientation at Ni(1)-Ni(2)-Ni(3)-Ni(4)	Magnetic moment	Magnitude $\mu_B$	Relative orientation at Ni(1)-Ni(2)-Ni(3)-Ni(4)
$\tilde{t}_y$	5.1	----	$m_x$	0.01	++--
$\tilde{q}_{xz}$	8.2	----	$m_y$	0	
$\tilde{a}$	5.7	+-+-	$m_z$	1.69	+-+-
$\tilde{q}_{x^2-y^2}$	0.3	+-+-			
$\tilde{q}_{z^2}$	5.9	+-+-			

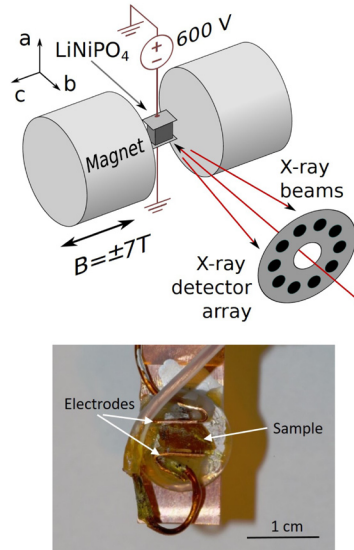


**Figure 2.** Experimental set up used to measure the antisymmetric Compton profile in  $\text{LiNiPO}_4$ . The upper panel shows a schematic of the experimental set up, with  $a$ ,  $b$  and  $c$  indicating the orientations of the crystal axes. The polar  $a$  axis was oriented vertically in the setup. A reversible magnetic field was applied along the crystal  $c$  axis. The  $b$  axis, which is the orientation of the  $\tilde{t}_y$  toroidal moment, was aligned close to the direction of photon momentum transfer, which defines the projection direction for the electron momentum density. The sample temperature was maintained at T~10K by the variable temperature stage of a helium-cooled superconducting magnet. The incident, linearly polarized x-ray beam of energy 184.3 keV passed through the aperture of a 10-element Ge detector, which subsequently measured the energy spectrum of the Compton scattered x-rays close to back-scattering. The lower panel is a photograph of the crystal on the sample holder with electrodes attached perpendicular to the  $a$ -axis (vertical in the picture).

field but opposite magnetic field. Field cooling with crossed electric and magnetic fields in this geometry should produce a single magnetoelectric domain state with its net magnetoelectric toroidal moment along the beam direction, as required for our experiment. Any incomplete domain alignment would result in a reduction in the signal.

During the experiment, the greatest practical challenge was arcing due to the high voltage and low pressure helium exchange gas environment. We were therefore only able to provide a high enough electric field for one polarity and with the magnetic field applied. We were then able to reverse the magnetoelectric domains by ramping the magnetic field, although this required long acquisition times of one hour per cycle period. During this time even small drifts in detector gain can lead to parasitic signals that had to be treated very carefully.

The energy spectrum of the measured inelastic scattering signal is, in general, easily mapped onto momentum space since the double differential cross-section is almost directly proportional to the Compton profile  $J(p_z)$  (see, for example, Ref. 23). Here, we were interested primarily in the antisymmetric difference profile, obtained by subtracting data sets measured with reversed magnetoelectric domains. Since there is a symmetry requirement for the two profiles to have the same area, the datasets were normalized prior to subtraction to ensure that this requirement was satisfied.

## IV. Results and discussion

### A. Density-functional theory results

Our calculated lowest-energy magnetic structure of  $\text{LiNiPO}_4$  has magnetic space group  $Pnm'a$ , consistent with experimental measurements. In this magnetic configuration, the magnetic moments at the Ni sites are anti-ferromagnetically arranged, with computed spin moment of  $1.69 \mu_B$  at each Ni site and zero net magnetization. The Ni spins are primarily oriented along the  $z$  direction with a small component along the  $x$  direction at each site, as a result of a small antiferromagnetic canting, as shown in Figure 1.

The magnetic  $Pnm'a$  symmetry of the ground state allows for various ME multipoles at the Ni sites, which have magnetic point group symmetry  $mm'm$ . These ME multipoles in turn have either ferro or anti-ferro type arrangements, as was pointed out previously in Ref. 2. In particular, the symmetry allows for toroidal moments along the  $y$  direction ( $t_y$ ) and  $q_{xz}$  quadrupole moment components, both with ferro-type arrangements, leading to a net  $t_y$  and  $q_{xz}$  in the system. In addition, the ME monopole  $a$  and the  $q_{x^2-y^2}$ ,  $q_z^2$  quadrupole moments are also allowed at the Ni sites. These multipoles have opposite signs at the neighboring Ni sites, however, leading to net zero contributions to  $a$ ,  $q_{x^2-y^2}$ , and  $q_z^2$ . Our density functional results for the ME multipoles are consistent with this symmetry analysis. The computed magnitudes of atomic-site contributions to the various allowed ME multipoles, and their relative orientations at different Ni sites are listed in Table II. As our calculation shows the presence of a net toroidal moment along the  $y$  direction, we expect an antisymmetric Compton profile along the same direction in momentum space<sup>15</sup>, which we now proceed to discuss.

We compute the Compton profile in the magnetic ground state of  $\text{LiNiPO}_4$  along the three Cartesian directions. In agreement with the expectation from symmetry arguments, we find an antisymmetric component in the Compton profile only along the  $y$  direction, which is the direction of the toroidal moment  $t_y$ , in momentum space. Our calculated total Compton profile  $J$  and the antisymmetric part,  $J^a$ , are depicted in Figure 3. Note that the antisymmetric contribution has been multiplied by  $10^3$ . We can see from this figure that the antisymmetric part of the profile is approximately four orders of magnitude smaller than the corresponding symmetric part of the profile. Although small, this signal should be at the limit of detectability, motivating the explicit measurements on  $\text{LiNiPO}_4$ , which we present in Section IV B.

Finally for this section, we analyze both parts of the profile to verify the zero-sum rules.

$$\int_{-\infty}^{\infty} p_y J^{s,a}(p_y) dp_y = 0 . \quad (3)$$

This is a trivial condition for the symmetric part  $J^s$  and is always satisfied because the integrand in Equation 3 is by definition always an odd function in  $p_y$ , resulting in a zero value upon integration. In contrast, for the antisymmetric part,  $J^a$ , the zero-sum rule imposes strict conditions on the positive- $p_y$  and negative- $p_y$  halves of the profile separately<sup>15</sup>, with

$$\int_{-\infty}^0 p_y J^a(p_y) dp_y = \int_0^{\infty} p_y J^a(p_y) dp_y = 0 . \quad (4)$$

We find that our computed antisymmetric Compton profile satisfies this condition to three decimal places.

### B. Experimental results and comparison with theory

In Figure 4 we show our measured total Compton profile (blue solid line with blue circles as data points) and the antisymmetric signal (red circles with error bars, multiplied by  $10^3$ ). The total profile is normalized so that the integral of the profile gives

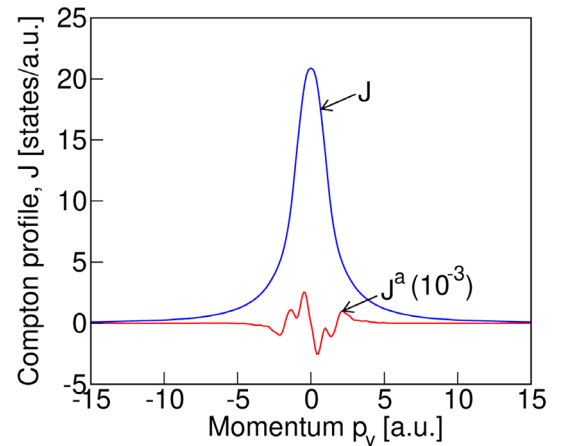


**Figure 3.** The computed (without convolution) total,  $J$ , and antisymmetric,  $J^a$ , Compton profile for the  $Pnm'a$  magnetic structure (see Figure 1 for the spin arrangement) of  $\text{LiNiPO}_4$ .

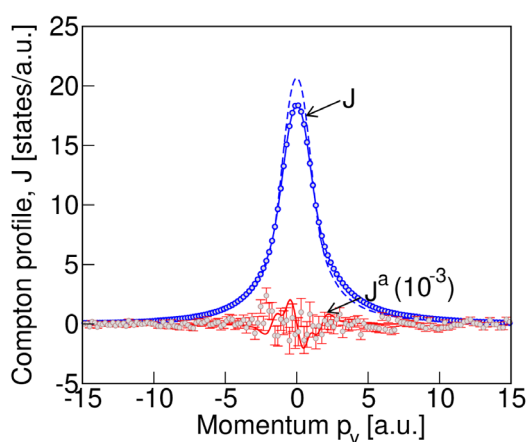


**Figure 4.** The measured Compton profile for  $\text{LiNiPO}_4$  compared with the calculated profile of Figure 3. The measured total Compton profile is shown by the blue circle data points and the blue solid line, while the measured antisymmetric profile, magnified by a factor of  $10^3$ , is indicated by the red circle data points and red vertical line error bars. The convoluted computed profiles with a Gaussian of FWHM = 0.44 from Figure 3 are shown as the blue dashed line (total profile) and red solid line (antisymmetric part of the calculated profile, magnified by a factor of  $10^3$ ). While the peak in computed total profile differs from the measured value by about 10% (see text for explanation), the measured and computed antisymmetric profiles are in the same orders of magnitude.

the total number of electrons in the unit cell of  $\text{LiNiPO}_4$  with four formula units. The antisymmetric profile is derived from the difference in Compton profiles measured in the presence of magnetic fields with opposite directions (see Equation 2). For comparison, the calculated profiles of Figure 3, after convolution with a Gaussian of full width at half maximum equal to our experimental resolution of 0.44 a.u., are also shown in Figure 4. The blue dashed line and red solid line depict the calculated convoluted total and antisymmetric profiles respectively. As seen from Figure 4, the peak in the calculated total profile is about 10% higher than the measured value. We also notice the skewness of the measured peak in the total Compton profile. We attribute both the skewness and the difference in measured and computed total profiles to multiple scattering effects, which are not considered here. The reason for ignoring the multiple photon scattering is that it does not have any significant contribution to the measured difference signal that was obtained by subtracting the data measured by reversing the magnetoelectric domains, as discussed in section III C. This is because although the multiple scattering contributes to the total Compton profile, when we take the difference in the data sets, measured with and without reversing the magnetoelectric domain, the multiple scattering contribution largely cancels out. Interestingly, we see that the data points corresponding to the measured antisymmetric signal are consistent with our calculated antisymmetric Compton profile, both being around four orders of magnitude smaller than the total profile. Frustratingly, however, both are at the level of the experimental noise (indicated by red error bars in Figure 4), and we are not able to conclusively infer the

existence of a non-zero antisymmetric contribution. Our analysis suggests that the experiment came very close to measuring a signal of the calculated magnitude and that a modest increase in experimental signal to noise ratio would likely have yielded a positive result.

## V. Summary

To summarize, we have studied the Compton profile in  $\text{LiNiPO}_4$ , the magnetic ground state of which allows for a net toroidal moment  $t_y$ . Our density functional calculations show the existence of an antisymmetric component in the Compton profile of  $\text{LiNiPO}_4$  along the same  $y$  direction in the momentum space as the toroidal moment, implicating antisymmetric Compton scattering as a possible signature of a time-odd, parity-odd ME toroidal moment  $t_y$  in the material. The calculated magnitude of the computed antisymmetric component is small, however, with magnitude  $\sim 10^{-4}$  times the calculated total Compton profile.

Our Compton scattering measurements on  $\text{LiNiPO}_4$  also find a weak difference signal, consistent with the computed order of magnitude. Unfortunately, however, the weak signal is of the same order of magnitude as the statistical error, preventing us from conclusively determining an antisymmetric profile.

Our finding that the predicted and measured antisymmetric Compton response of  $\text{LiNiPO}_4$  is exactly at the noise level motivates further research in two directions: First, materials with a larger antisymmetric Compton profile should be identified, so that existing experiments will provide an unambiguous signal. Second, since the experimental signal to noise ratio was limited by the detector count-rate capability, solid angle, incident beam flux and monochromator bandwidth, optimization of these factors, while practically challenging, could improve the signal to noise by an order of magnitude, allowing anti-symmetric Compton profiles to be determined with ease.

## Data availability

### Underlying data

The experimental data is available as follows:

Zenodo: Anti-symmetric Compton scattering in  $\text{LiNiPO}_4$ : Towards a direct probe of the magneto-electric multipole moment. <https://doi.org/10.5281/zenodo.5167599>

This project contains the following experimental files:

- Data file description.docx: Description of data files
- data.zip: Experimental data files
- photos.zip: Photographs from the experiment
- evernote log electronic logbook.pdf: Electronic logbook for the experiment
- SPring-8 antisymmetric compton proposal may 2017.pdf: Beamtime proposal

The theoretical data is available as follows:

Materials Cloud: Anti-symmetric Compton scattering in  $\text{LiNiPO}_4$ : Towards a direct probe of the magneto-electric multipole moment. <https://doi.org/10.24435/materialscloud:yx-7k>

The description of the files and folders for this project is the following:

- The main folder “data” contains the two separate folders, “ $3 \times 6 \times 6$ ” and “ $5 \times 10 \times 10$ ” corresponding to the two different k-grids, used for the theoretical calculations of the Compton profile in  $\text{LiNiPO}_4$ . Each folder contains all the input files necessary for reproducing our results, and the output data files for the theoretical

Compton profile, that are presented in the paper. The folder “ $3 \times 6 \times 6$ ” contains the sub-folder “fig3-data-files” that includes the explicit data files corresponding to the theoretical plots in Figure 3 of the paper.

Data are available under the terms of the [Creative Commons Attribution 4.0 International license](#) (CC-BY 4.0).

## Acknowledgements

Calculations were performed on the ETH Zürich Euler cluster. The synchrotron radiation experiments were performed at SPring-8 BL08W with the approval of the Japan Synchrotron Radiation Research Institute (JASRI) (Proposal No. 2018A1091).

## References

1. Spaldin NA, Fiebig M, Mostovoy M: **The toroidal moment in condensed-matter physics and its relation to the magnetoelectric effect.** *J Phys: Condens Matter*. 2008; **20**(43): 434203. [PubMed Abstract](#) | [Publisher Full Text](#)
2. Spaldin NA, Fechner M, Bousquet E, et al.: **Monopole-based formalism for the diagonal magnetoelectric response.** *Phys Rev B*. 2013; **88**(9): 094429. [PubMed Abstract](#) | [Publisher Full Text](#)
3. Spaldin NA: **ANALOGY BETWEEN THE MAGNETIC DIPOLE MOMENT AT THE SURFACE OF A MAGNETOELECTRIC AND THE ELECTRIC CHARGE AT THE SURFACE OF A FERROELECTRIC.** *J Exp Theor Phys*. 2021; **159**: 594–597. [PubMed Abstract](#) | [Publisher Full Text](#)
4. Schmid H: **Magnetoelectric Effects in Insulating Magnetic Materials.** (edited by W. S. Weighogher and A. Lakhtakia (SPIE Press, Bellingham, WA), 2003; 167–195. [PubMed Abstract](#) | [Publisher Full Text](#)
5. Van Aken BB, Rivera JP, Schmid H, et al.: **Observation of ferrotoroidic domains.** *Nature*. 2007; **449**(7163): 702–705. [PubMed Abstract](#) | [Publisher Full Text](#)
6. Arima TH, Jung JH, Matsubara M, et al.: **Resonant Magnetoelectric X-ray Scattering in  $\text{GaFeO}_3$ : Observation of Ordering of Toroidal Moments.** *J Phys Soc Jpn*. 2005; **74**(5): 1419–1422. [PubMed Abstract](#) | [Publisher Full Text](#)
7. Staub U, Bodenthin Y, Piamonteze C, et al.: **Parity- and time-odd atomic multipoles in magnetoelectric  $\text{GaFeO}_3$  as seen via soft x-ray Bragg diffraction.** *Phys Rev B*. 2009; **80**(14): 140410. [PubMed Abstract](#) | [Publisher Full Text](#)
8. Lovesey SW: **Magneto-electric operators in neutron scattering from electrons.** *J Phys Condens Matter*. 2014; **26**(35): 356001. [PubMed Abstract](#) | [Publisher Full Text](#)
9. Staub U, Bodenthin Y, Piamonteze C, et al.: **Magnetoelectric effects studied by resonant x-ray diffraction in ferrimagnetic  $\text{GaFeO}_3$ .** *Phys Rev B*. 2010; **82**(10): 104411. [PubMed Abstract](#) | [Publisher Full Text](#)
10. Scagnoli V, Staub U, Bodenthin Y, et al.: **Observation of Orbital Currents in  $\text{CuO}$ .** *Science*. 2011; **332**(6030): 696–698. [PubMed Abstract](#) | [Publisher Full Text](#)
11. Kubota M, Arima T, Kaneko Y, et al.: **X-Ray Directional Dichroism of a Polar Ferrimagnet.** *Phys Rev Lett*. 2004; **92**(13): 137401. [PubMed Abstract](#) | [Publisher Full Text](#)
12. Sessoli R, Boulon ME, Caneschi A, et al.: **Strong magneto-chiral dichroism in a paramagnetic molecular helix observed by hard X-ray.** *Nat Phys*. 2015; **11**(1): 69–74. [PubMed Abstract](#) | [Publisher Full Text](#) | [Free Full Text](#)
13. Jung JH, Matsubara M, Arima T, et al.: **Optical Magnetoelectric Effect in the Polar  $\text{GaFeO}_3$  Ferrimagnet.** *Phys Rev Lett*. 2004; **93**(3): 037403. [PubMed Abstract](#) | [Publisher Full Text](#)
14. Ederer C, Spaldin NA: **Towards a microscopic theory of toroidal moments in bulk periodic crystals.** *Phys Rev B*. 2007; **76**(21): 214404. [PubMed Abstract](#) | [Publisher Full Text](#)
15. Collins SP, Laundry D, Connolly T, et al.: **On the possibility of using X-ray Compton scattering to study magnetoelectrical properties of crystals.** *Acta Crystallogr A Found Adv*. 2016; **72**(Pt 2): 197–205. [PubMed Abstract](#) | [Publisher Full Text](#) | [Free Full Text](#)
16. Mercier M, Bauer P: *Acad Sci Paris*. 1968; **267**: 465.
17. Jensen TBS, Christensen NB, Kenzelmann M, et al.: **Field-induced magnetic phases and electric polarization in  $\text{LiNiPO}_4$ .** *Phys Rev B*. 2009; **79**(9): 092412. [PubMed Abstract](#) | [Publisher Full Text](#)
18. Fogh E, Kihara T, Toft-Petersen R, et al.: **Magnetic structures and quadratic magnetoelectric effect in  $\text{LiNiPO}_4$  beyond 30 T.** *Phys Rev B*. 2020; **101**(2): 024403. [PubMed Abstract](#) | [Publisher Full Text](#)
19. Abrahams I, Easson KS: **Structure of lithium nickel phosphate.** *Acta Cryst*. 1993; **49**: 925–926. [PubMed Abstract](#) | [Publisher Full Text](#)
20. **The Elk Code.** [Reference Source](#)
21. Ernsting D, Billington D, Haynes TD, et al.: **Calculating electron momentum densities and Compton profiles using the linear tetrahedron method.** *J Phys Condens Matter*. 2014; **26**(49): 495501. [PubMed Abstract](#) | [Publisher Full Text](#)
22. Biggs F, Mendelsohn LB, Mann JB: **Hartree-Fock Compton profiles for the elements.** *Atomic Data and Nuclear Data Tables*. 1975; **16**(3): 201–309. [PubMed Abstract](#) | [Publisher Full Text](#)
23. Cooper MJ: **Compton scattering and electron momentum determination.** *Rep Prog Phys*. 1985; **48**(4): 415. [PubMed Abstract](#) | [Publisher Full Text](#)
24. Bhowal S, O'Neill D, Fechner M, et al.: **Anti-symmetric Compton scattering in  $\text{LiNiPO}_4$ : Towards a direct probe of the magneto-electric multipole moment.** [Data set]. Zenodo. 2021. [PubMed Abstract](#) | [Publisher Full Text](#)
25. Bhowal S, O'Neill D, Fechner M, et al.: **Anti-symmetric Compton scattering in  $\text{LiNiPO}_4$ : Towards a direct probe of the magnetoelectric multipole moment.** *Materials Cloud Archive* 2021.119. 2021. [PubMed Abstract](#) | [Publisher Full Text](#)

# Open Peer Review

Current Peer Review Status: 

Version 1

Reviewer Report 22 November 2021

<https://doi.org/10.21956/openreseurope.14947.r27944>

© 2021 Nordstrom L. This is an open access peer review report distributed under the terms of the [Creative Commons Attribution License](#), which permits unrestricted use, distribution, and reproduction in any medium, provided the original work is properly cited.



Lars Nordstrom 

Department of Physics and Astronomy, Uppsala University, Uppsala, Sweden

- This report is on a combined theoretical and experimental study on the anti-symmetric Compton scattering on a magneto-electric material LiNiPO<sub>4</sub> in the strive to observe local toroidal moments.
- As is clearly stated in the manuscript the conclusions are not strictly conclusive as the experimental error bars are of the same order as the variations in the detected signal. However, it is on the other hand not contradicting the theoretical study.
- The report outlines the way to proceed in future studies to study local magnet-electric moments where the experimental resolution can be increased.
- This study is sound and honest and deserves indexing.

**Is the work clearly and accurately presented and does it cite the current literature?**

Yes

**Is the study design appropriate and does the work have academic merit?**

Yes

**Are sufficient details of methods and analysis provided to allow replication by others?**

Yes

**If applicable, is the statistical analysis and its interpretation appropriate?**

Yes

**Are all the source data underlying the results available to ensure full reproducibility?**

Yes

**Are the conclusions drawn adequately supported by the results?**

Yes

**Competing Interests:** No competing interests were disclosed.

**Reviewer Expertise:** My expertise is corresponding to the theoretical side of this study. Especially regarding the local multipoles of magnetically ordered materials, not least in systems which are both correlated and relativistic.

**I confirm that I have read this submission and believe that I have an appropriate level of expertise to confirm that it is of an acceptable scientific standard.**

-----